Electronic Supplementary Material (ESI) for Lab on a Chip.

Electronic Supplementary Information

Wettability patterning for high-rate, pumpless fluid transport on open, non-planar microfluidic platforms

Aritra Ghosh,[a] Ranjan Ganguly,[a,b] Thomas M. Schutzius,[a,c] Constantine M. Megaridis[a]

[a] *Department of Mechanical and Industrial Engineering, University of Illinois at Chicago, Chicago, IL 60607, USA*

[b] *Department of Power Engineering, Jadavpur University, Kolkata 700098, India*

[c] *Department of Mechanical and Process Engineering, ETH Zürich, 8092 Zürich, Switzerland*

S1. Surface wettability characterization (Section 2)

Contact angle measurements were performed on the bare and coated (superhydrophobic and superhydrophilic parts) aluminum, paper and PET substrates. Both aluminum and paper exhibited sessile contact angles slightly less than 90°. The PET substrate showed strong wettability (apparently due to a commercial coating on the transparency film used in the experiment).

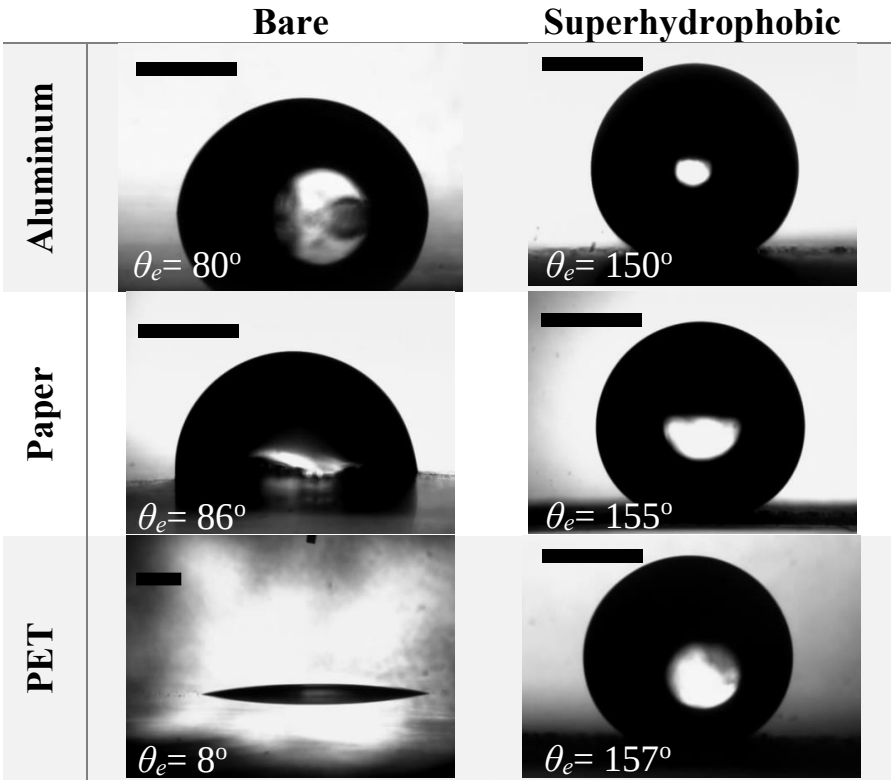

Figure S1: Sessile droplets on the bare substrate (left) and superhydrophobic sections (right) of aluminum, paper and PET substrates. This figure shows one sample image for each substrate taken from several runs used to obtain the θ_e data listed in Table 1. Each scale bar denotes 1mm.

S2. Variation of capillary force on droplet with wedge angle α and liquid volume Ω (Section 3.1)

To confirm the validity of Eq. (2), which indicates that the Laplace pressure gradient on a droplet placed on the wedge-shaped track is proportional to the wedge angle –as long as α is small– we carried out a separate experiment (see Fig. 3(a)) for evaluating the capillary force on the droplet as it began its journey from the narrow end on the track. The experiment was repeated for wedge angles of 0, 2, 3, 4 and 5 degrees. The superhydrophilic tracks were presuffused with water and droplets of known volumes were deposited. The substrates were initially tilted with the wider end up at an angle steep enough so that the forward (i.e., up-slope) capillary force on the liquid bulge could not overcome its in-plane component of weight (acting down-slope), thus keeping the droplet pinned at the narrower

end of the track (Fig S2(a)). Inclination (β) of the substrate was very slowly decreased until the in-plane component of the droplet weight became lower than the capillary force and the droplet started moving up the plane (Fig. S2(b)). For rectangular tracks ($\alpha = 0^o$) the liquid bulge deposited on the track did not move (although capillary spreading of the liquid front was observed) even for $\beta = 0$ (horizontal surface). For higher wedge angles, the inclination β marking the impending motion of droplets was also higher, implying that the capillary force increased with α. The capillary force on the liquid bulge, as Eq. (2) suggests, also depends on θ_{avg}, which should be a function of the dispensed droplet volume Ω. In order to explore this dependence, we deposited droplets ranging from 4.7 ï 23.5 μl and recorded the corresponding values of β. Figure S2(c) shows the variation of capillary force F_{cx} with droplet volume Ω for different wedge angles. Each data point was obtained from averaging 60 to 300 readings, while the error bars denote the standard deviation in these readings. For larger wedge angles ($\alpha = 4^o$ and 5^o) the capillary force was too strong to be countered by the weight of small volume droplets, and hence only larger volumes of droplet had to be dispensed. For all the substrates, the droplet volume was found not to influence the capillary force strongly. Therefore, the average F_{cx} values of Fig. 3(b) were plotted using the data sets for each value of α in Fig. S2(c) by averaging over the entire range of droplet volumes used for each α.

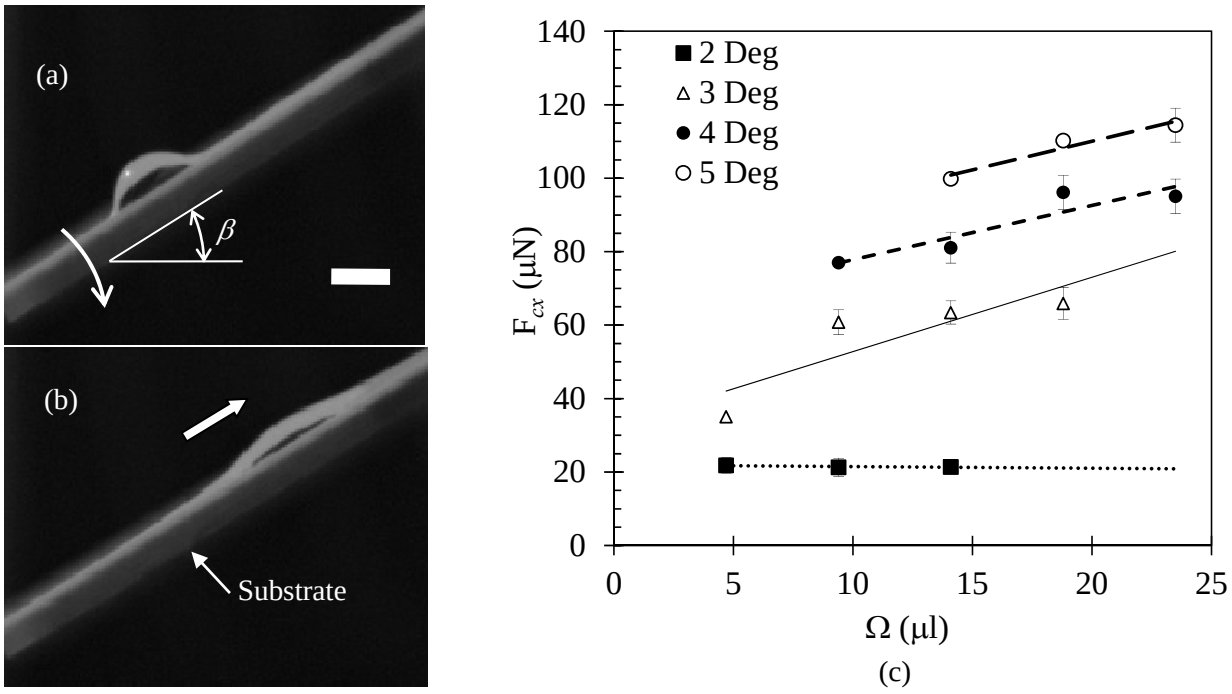

Figure S2: Image of the liquid accumulation on the inclined wedge track (a) just before β reached the critical value below which the liquid bulge started moving up the plane, as shown in (b). (c) Variation of the capillary force on the droplet with droplet volume for different values of wedge angle α. Scale bar denotes 2 mm.

S3. Holding capacity of a wedge track (Section 3.1)

For an isolated superhydrophilic wedge track of finite length on a superhydrophobic background, liquid that is transported from the narrow to the wide end remains confined in the track. If the track is wide enough, the liquid builds up initially creating a rising rivulet from the narrow to the wide end. Further addition of liquid shows that the track retains its pumping ability, with the accumulating height increasing further. When Ω/δ^3 exceeds a critical value, a liquid bulge becomes wider that the wide end of the track. For a track of 60 mm length and 4° wedge angle the wider end measures $\delta \sim 4.2$ mm; the bulge at the wide end did not evolve until 50 droplets of 4.7 μL each were deposited at the narrow end and transported there, leading to $\Omega/\delta^3 = \left(235/4.2^3\right) = 3.17$ (see Fig. S3).

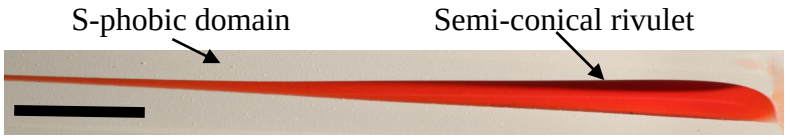

Figure S3: Image of the liquid accumulated after approximately 235 μL of water (dyed for better visualization) were dispensed at the left end of the track. Scale bar denotes 10 mm.

S4. Effect of pre-wetting (presuffusing) the track (Section 3.1)

Supplementary movie SM1 shows the transport of water droplet on a 4^{o} wedge track; the movie is played at 1/30th of its real-time speed. In the movie, the droplet was intentionally pinned to the dispensing needle for about two seconds (when its lower end touched the track) to allow a presuffusing front to proceed visibly ahead of the liquid pool (see the ~ 3.5 mm dark presuffused track in the movie at its opening frame). Figure S4 shows the effect of presuffusing on the capillary pore diameter that is driving hemiwicking. For a dry track, hemiwicking speed is limited by the smallest (deepest) roughness features on the surface. On a presuffused track, these smallest features are already submerged in liquid, leaving larger length-scale features, which in turn limit the hemiwicking speed. Since the latter scales linearly with pore diameter, liquid velocity is higher on the presuffused track.

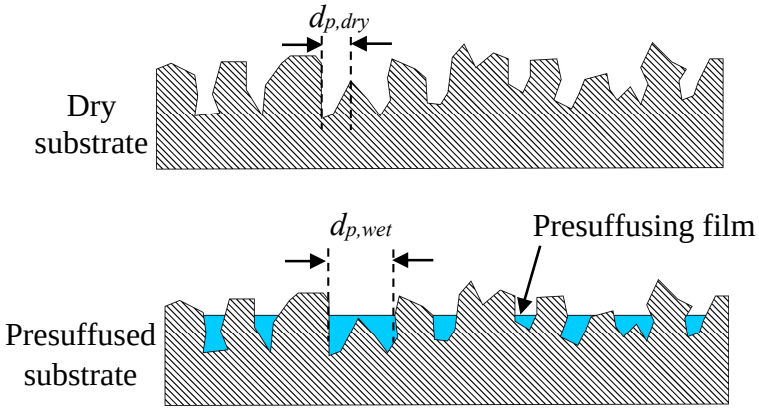

Figure S4: Effect of presuffusing on liquid mobility: for a dry track (top) the smaller surface features (characteristic dimension $d_{p,dry}$) limit the hemiwicking speed. For a presuffused track (bottom), the narrower crevices of the tracks are submerged, and the hemiwicking speed is limited by the relatively larger features ($d_{p,wet}$) of the exposed surface roughness.

S5. Evaluation of droplet acceleration at $t = 0$ (Section 3.1)

Figure S5 shows the velocity of the liquid bulge as a function of time as it moved along the presuffused track with $\alpha = 3^o$; see Fig. 4(a) for the corresponding x vs. t plot. As discussed in the main text, the liquid bulge starts from rest due to its inertia. A cubic polynomial fit indicates that the acceleration of the liquid bulge at the inception of the droplet motion was $\mathrm{d}V/\mathrm{d}t\big|_{t=0} = 12.3$ m/s^2. This matches closely with the acceleration (12 m/s^2) measured for a 4.7 μL droplet that was driven by a capillary force of 56.3 μN (see Fig. 3(b)) on a tilted surface.

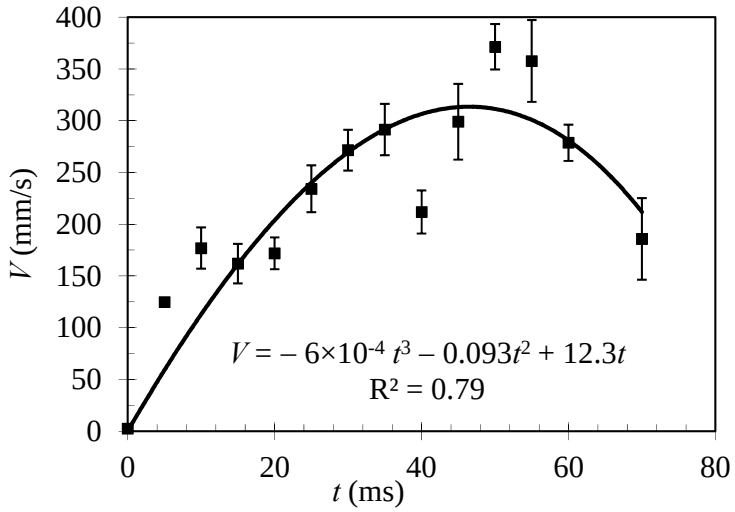

Figure S5: Velocity-time plot of the liquid bulge on a horizontal presuffused track with $\alpha = 3^o$.

S6. Capillary bridging (Section 3.2.1)

Capillary bridging of the liquid bulges at the wider ends of tracks A and B took place where the surfaces of the two bulges touched (see supplementary movie SM2). The bridge formed in the air (i.e., the liquid bridge does not touch the substrate at $t = 0$) with an initial thickness h_0. The two adjacent bulges, which remained pinned to the superhydrophilic tracks, coalesced through progressive growth of the liquid bridge. The width h of the capillary bridge (as seen from the end view reported in Fig. 5(b1) ï (e1)) is plotted in Fig. S6 for four different runs. The growth rate h/h_0 was found to scale with $t^{1/2}$, which is typical of inertia-dominated coalescence (for viscous flow the dependence would have been proportional to t).[1]

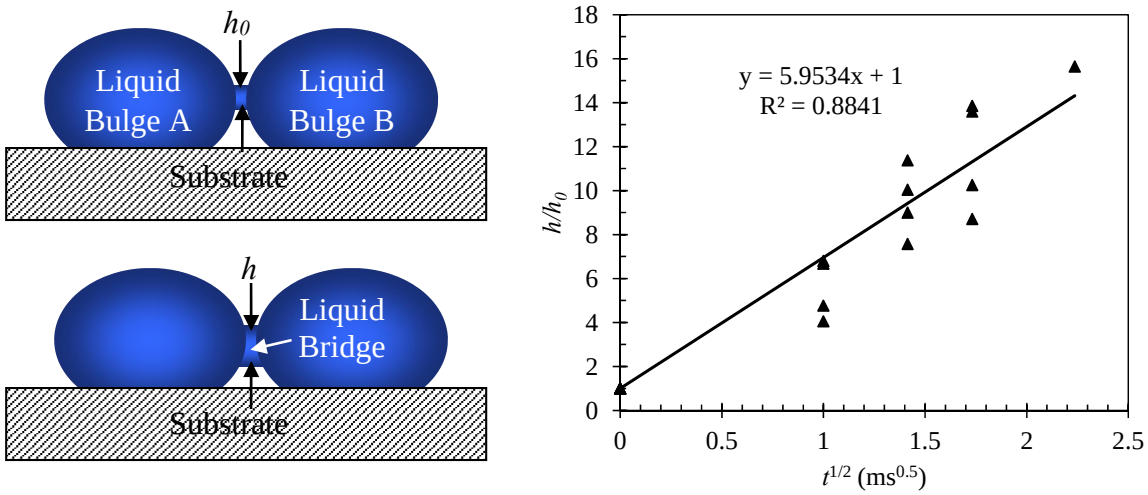

Figure S6: Growth of the capillary bridge thickness (normalized with h_0, the initial bridge thickness) as measured from Figs. 5(b1 ï e1) as a function of time. The bridge height exhibits a linear dependence with $t^{1/2}$ (time scale is in milliseconds).

S7. Droplet splitting on paper and PET films (Section 3.2.2)

Like the droplet bridging circuit (Section 3.2.1), the droplet splitter design also worked equally well on paper and PET substrates. Figure S7(a) shows the images of the three-track design on paper, while Fig. S7(b) and (c) show the images of the split volumes of water (colored for visualization) after dispensing 5 (23.5 µL) and 15 droplets (70.5 µL), respectively.

To demonstrate how any eccentricity or bias in the position of the liquid dispenser leads to unequal degrees of liquid distribution along the splitter limbs, we dispensed 5 droplets (23.5 µL) with an offset of ~100 µm from the center spot. Figure S7(b) shows the extent of the resulting unequal liquid distribution. Figure S7(c1ï c4) shows droplet splitting in a 5-splitter design on PET film. The bridged droplet at the early stage of splitting can be seen in frame (c2), while frame (c3) shows the nearly even distribution of the liquid after the split is complete. The central spot can be seen to retain a very small volume. The splitting continues for several consecutive droplets released until the accumulated liquid volume in the radial tracks eventually deters the de-bridging of the central droplet at the end of pumping. Figure S7(c4) shows the liquid accumulation at the end of splitting of 10 consecutive droplets (47 µL). This particular design on PET film has been found to work with repeatable features up to 17 consecutive splitting droplets (~80 µL) (see supplementary movie SM3).

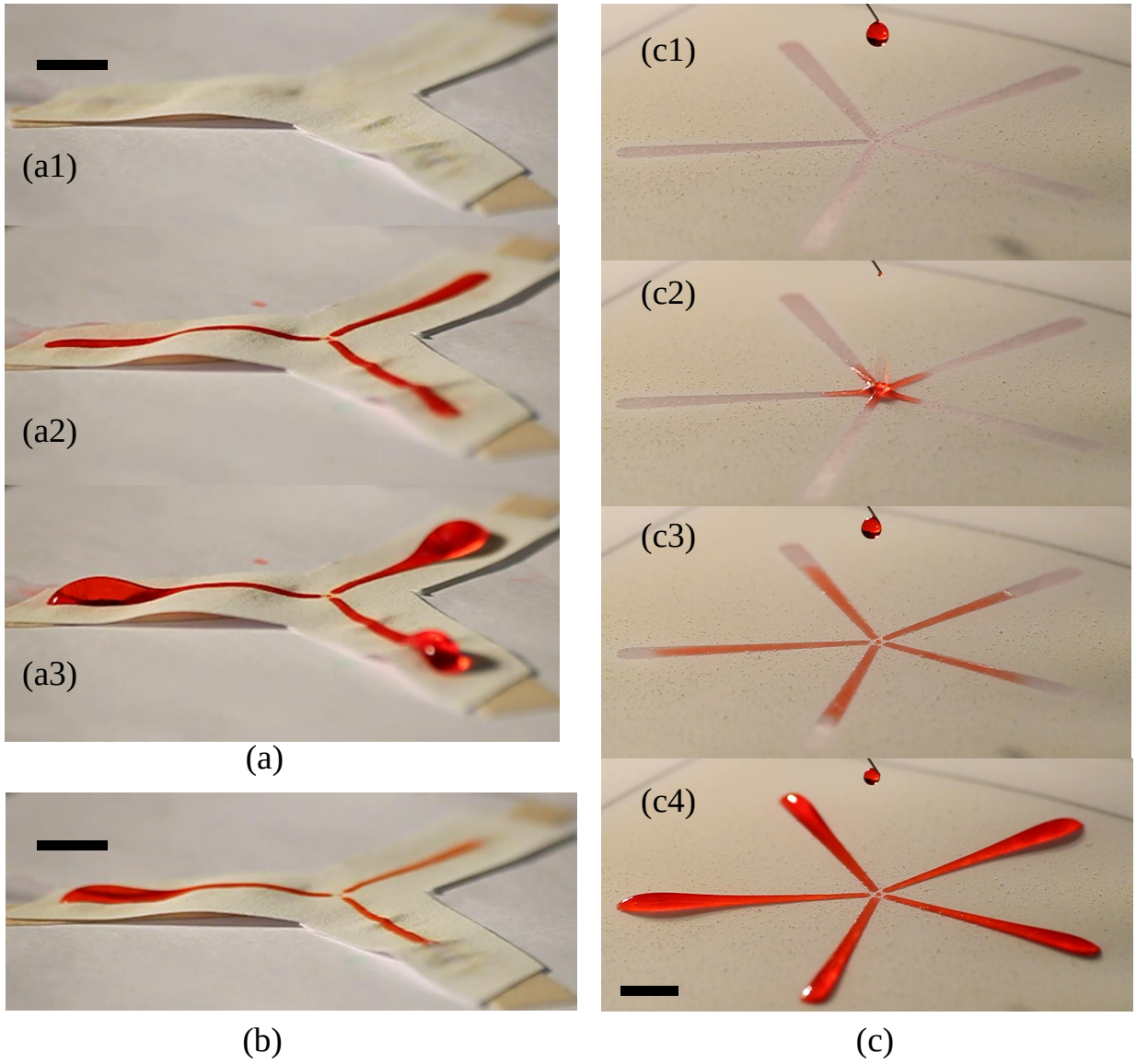

Figure S7: (a - b) Three-way droplet splitting on a paper substrate. (a1) The substrate, (a2) liquid accumulation after perfectly symmetric deposition of 5 drops (23.5 µL) at the center, (a3) same, after 15 drops (70.5 µL). (b) Biased accumulation after asymmetric splitting of 5 successively dispensed droplets. (c) Five-way droplet splitting on transparency (PET) film: (c1 ï c3): sequence of the first droplet split, (c4) liquid accumulation after splitting of 10 droplets (47 µL). Scale bars denote 5 mm.

List of Supplementary Movies (SM):

1. High-speed movie of a 4.7 μL droplet transported on a wedge track (recorded at 1000 fps, played at 30 fps) on Al-substrate (see Section 3.1).
2. High-speed movie of liquid bridging, transport and de-bridging (recorded at 1000 fps, played at 30 fps) on Al-substrate (refer to Fig. 5).
3. Droplet splitting on PET substrate (refer to Fig. S7(c)).
4. Liquid transport up a 13^{o} ramp on PET substrate (refer to Fig. 8).

References

1 D.G.A.L. Aarts, H.N. W. Lekkerkerker, H. Guo, G.H. Wegdam and D. Bonn, *Phys. Rev. Lett.*, 2005, **95**, 164503.